Title

Co2+ acireductone dioxygenase: Fe2+ mechanism, Ni2+ mechanism, or something else?

Authors

Valdez, Crystal E
Gallup, Nathan M
Alexandrova, Anastassia N

Publication Date

2014-06-01

DOI

10.1016/j.cplett.2014.04.055

Peer reviewed

Chemical Physics Letters 604 (2014) 77–82

Contents lists available at ScienceDirect

Chemical Physics Letters

journal homepage: www.elsevier.com/locate/cplett

Co^{2+} acireductone dioxygenase: Fe^{2+} mechanism, Ni^{2+} mechanism, or something else?

Crystal E. Valdez [a], Nathan M. Gallup [a], Anastassia N. Alexandrova [a,b,*]

[a] Department of Chemistry and Biochemistry, University of California, Los Angeles, Los Angeles, CA 90095-1569, USA
[b] California NanoSystems Institute, 570 Westwood Plaza, Building 114, Los Angeles, CA 90095, USA

ARTICLE INFO

Article history:
Received 10 April 2014
In final form 29 April 2014
Available online 9 May 2014

ABSTRACT

Acireductone dioxygenase (ARD) oxidizes 1,2-dihydroxy-3-keto-5-(methylthio)pentene to either formate and an α-keto acid, or formate, methylthiopropionate and CO, depending on the nature of the catalytic metal, Fe^{2+} or Ni^{2+}. We recently showed that, contrary to established hypotheses, the mechanistic preference is driven solely by the RedOx behavior of the metal. Here, we address the functionality of Co^{2+}-ARD. Using mixed quantum–classical dynamics simulations and density functional theory calculations, we show that both Fe^{2+}-like and Ni^{2+}-like routes are accessible to Co^{2+}-ARD, but the mechanism involves a bifurcating transition state, and so the exact product distribution would be determined by the reaction dynamics.

1. Introduction

Metalloenzymes carry out a broad and diverse range of biological functions such as nitrogen fixation, metabolism, respiration, photosynthesis and oxygen transport [1]. It is often still a mystery why nature chooses specific metals for catalysis. Acireductone dioxygenases (ARD and ARD′) is a monometallic enzyme involved in the methionine salvage pathway in living organisms, including humans [2–5]. ARD oxidizes the substrate 1,2-dihydroxy-3-keto-5-(methylthio)pentene (acireductone) using dioxygen. Interestingly, the nature of the bound metal is the exclusive determinant of whether the products are recycled or excreted in the methionine salvage pathway. Fe-ARD′ (EC 1.13.11.54) oxidizes acireductone into two products, formate and 2-keto-4-methylthiobutyric acid, the precursor of methionine, and then continues along the metabolic pathway. Ni-ARD (EC 1.13.11.53) catalyzes the formation of formate, methylthiopropionate and carbon monoxide, which exit the pathway. Through a theoretical study, the reaction pathway differentiation was found to be solely due to the electronic properties of the metal, disproving previous speculations that the binding mode of the substrate to the metal center dictated the mechanism (Figure 1) [2]. Fe-ARD′ has an additional intermediate on the reaction profile, where the dioxygen attached to the substrate is dissociated. For Ni-ARD, dioxygen is activated but remains bound. This contrasting behavior is the result of the greater RedOx flexibility of the Fe^{2+} cation: having more holes in the 3d-set of atomic orbitals, Fe^{2+} efficiently transmits electrons from its ligands to the bound substrate and dioxygen molecule, causing its dissociation. The split-dioxygen intermediate is prone to oxygen migration, leading to the Fe-ARD′ products. Ni^{2+} has the 3d-set nearly full, and does not act as an analogous electron pump. Thus, the effect of just two extra electrons in the metal in ARD on the mechanism of reaction is dramatic. If to consider the nature of the metal as a means to tune the catalysis by metallo-enzymes, ARD represents a curious case.

In this work we assess the catalytic mechanism Co^{2+}-ARD. Would Co-ARD follow the Fe-ARD′ pathway, Ni-ARD pathway, or a completely different pathway? Co is a vital metal in biology [6,7], found, for example, in cobalamin, commonly known as vitamin B12 [8], carbonic anhydrase [9], and blue copper proteins [10]. In ARD, Co is not found naturally, but can be installed by ion exchange. Experimentally, when ARD is reconstituted with Co, it has been found to form primarily Ni products [11,12], however the mechanistic details are not elucidated. In view of the exemplary sensitivity of the ARD enzyme to the electronic structure of the metal, we are interested to see how the Co-ARD mechanism unfolds and compares to the two native forms of the enzyme.

2. Theoretical methods

The initial structure of ARD was obtained from the Protein Data Base (PDB) (code: 2HJI [13]). 2-Dihydroxy-3-keto-5-methylthiopentene was manually docked into the protein, with O1 and O3 being deprotonated and positioned in a six-membered ring relative

* Corresponding author at: Department of Chemistry and Biochemistry, University of California, Los Angeles, Los Angeles, CA 90095-1569, USA.
E-mail address: ana@chem.ucla.edu (A.N. Alexandrova).

http://dx.doi.org/10.1016/j.cplett.2014.04.055
0009-2614/

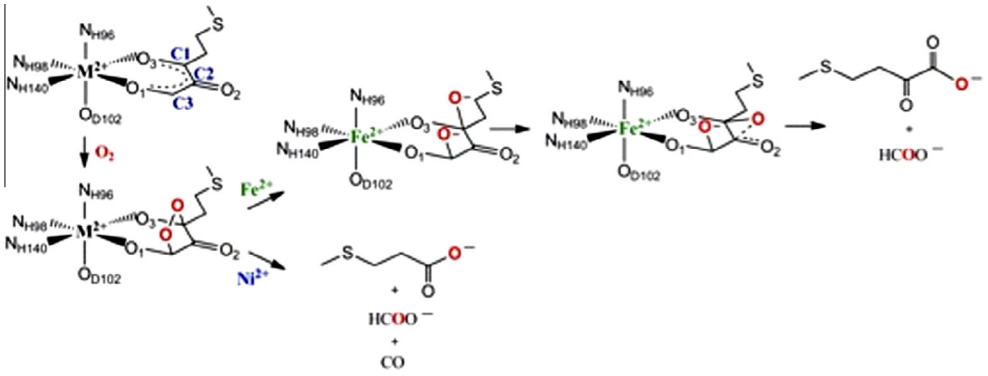

Figure 1. The mechanism of acireductone oxidation in ARD and ARD′, where the additional 'split-dioxygen' intermediate found in ARD′ differentiates the two pathways.

to the equatorial plane of the Co complex, in accord with experimental and theoretical predictions for other metal forms of ARD [14–16] (Figure 2A). Previous QM/DMD simulations on the Fe-ARD′ and Ni-ARD systems elucidated the need for adequate sampling of the backbone and substrate since the two residues, R104 and R154, were found to form vital hydrogen bonds with the substrate and active site [2], to stabilize the doubled deprotonated substrate and the six-membered ring orientation of the substrate to the metal.

This study utilizes our developed mixed quantum mechanical/discrete molecular dynamics [17–21] (QM/DMD) [21] method. QM/MM is a typical approach to studies of metalloenzymes [22]. QM/DMD is a hybrid method that efficiently captures metalloprotein dynamics with a quantum mechanical description of the active site on the order of tens to hundreds of nanoseconds. DMD differs from traditional molecular dynamics (MD) by the interaction potential functions, where the continuous potential functions are approximated with step functions of pairwise distances. This reduces DMD to event-drive MD simulations where a non-traditional time unit (t.u.) is introduced and defined as the shortest time between two consequent collisions in the system between two points. DMD has been utilized extensively on biomolecule systems such as the one in this study [17–20]. Examples of the capabilities of QM/DMD include comprehensive mechanistic studies of enzymatic reactions [23], unveiling the subtle structural details at metal-containing active sites [24] and proficient protein conformational responses to metal replacement and substrate binding [25]. The affordability of QM/DMD is the key attractive quality of the method when compared to equally capable QM/MM methods.

Details of the QM/DMD method are described elsewhere [21]. Briefly, QM/DMD operates in an iterative scheme with three well defined regions – the QM-only, DMD-only and the QM-DMD boundary. First, DMD samples most of the protein, excluding the exclusively QM-only region – the metal and atoms directly coordi-

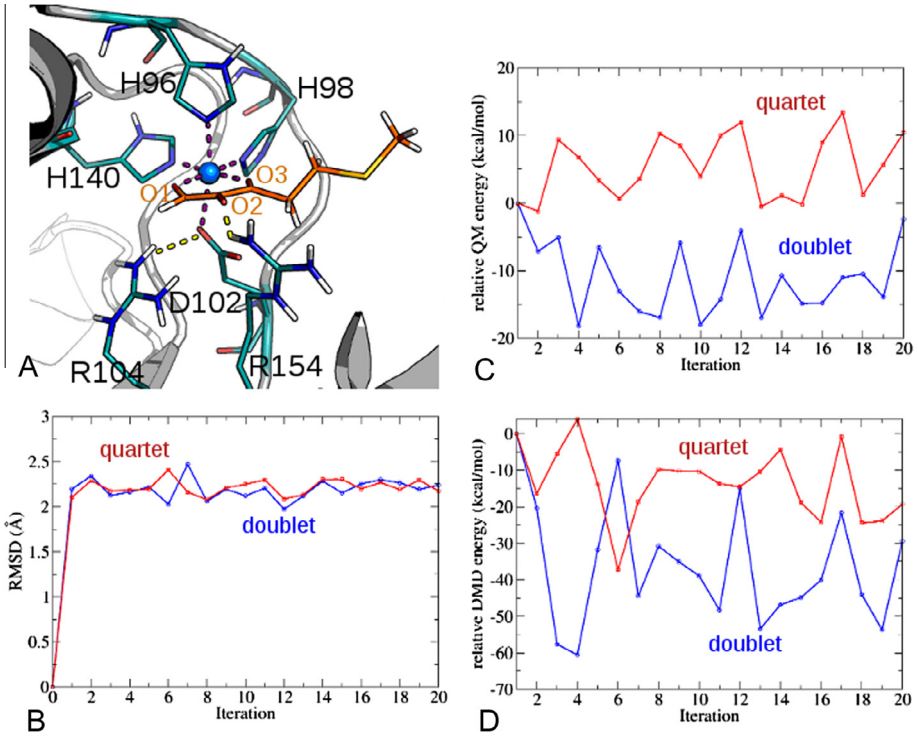

Figure 2. (A) The QM-DMD boundary in the protein is colored teal and includes residues H96, H98, D102 and H140 that directly coordinate the metal, the Co^{2+} metal, the substrate (orange) and R104 and R154, residues found to be important in stabilizing the dianionic substrate. Parts (B–D) who the convergence data from QM/DMD simulations for the doublet (blue lines) and quartet (red lines): (B) the backbone RMSD shows overall stabilization of the protein structure; (C) and (D) are the relative QM and DMD energies. (For interpretation of the references to color in this figure legend, the reader is referred to the web version of this article.)

nated to the metal (N from His, O from Glu and O1 and O3 of the substrate). This allows us to avoid force field parameterization for the metal. Following DMD, the extended QM region is extracted from the protein and goes through a geometry optimization, following the *ab initio* gradients of the larger active site that includes the metals, ligands, the substrate, and R104 and R154. Through the 'breathing' QM/DMD boundary, the DMD and QM regions communicate with one another (Figure S1). QM/DMD is pleasantly insensitive to abrupt changes on the potential at the QM-DMD boundary, since we never calculate forces there, due to the nature of DMD. Note, however, that for this same reason fairly large fluctuations in QM and DMD energies are typical for complexes as large as the studied QM/DMD region [23–25]. Since Co is found in both low and high spin states in nature [8–10], two sets of QM/DMD simulation were run for the two different spin states of Co.

2.1. QM/DMD partitioning scheme

The QM-only, DMD-only and QM–DMD boundary are all depicted in Figure 2. The QM-only domain includes the Co^{2+} ion, NE2 of H96, H98 and H140, OE1 of E102 and the two deprotonated oxygens (O1 and O3) of the substrate. The QM–DMD boundary includes the remaining atoms of residues H96, H98, H140, E102, the substrate, and R104 and R154. The amino acids in the QM optimization are chopped at the Cα–Cβ bond, Cδ–Cγ for arginines, and saturated with hydrogens. The hydrogens are positioned along the original bond at a distance equal to 0.7052*R(C–C/N). All saturated hydrogens and their bond partners are frozen during the QM optimization to retain the protein scaffold geometry. During DMD, further constraints are imposed to prevent any residues coordinating the metal from losing their coordination with the metal. DMD is allowed to sample those constrained atoms only within ±0.01 Å from the QM values. These constraints have been shown to not hinder important sampling movement of the protein [21].

2.2. Details of the simulations

Each simulation begins with a short DMD run of 1000 DMD time units (t.u.) (~50 fs) at a DMD temperature of 0.1 kcal/mol K, with a high heat exchange rate of the protein with the bath for 10 $t.u.^{-1}$, using the Andersen thermostat [26]. This short DMD simulation with high heat exchange was found to remove clashes introduced from pdb starting structures. Following the removal of clashes, a simulated annealing procedure is performed, shown to be crucial for avoiding local minimum traps during sampling and achieve better statistics of the resulting ensemble [21]. The annealing equilibration peaks at a temperature of 0.2 kcal/mol K and, in 0.02 kcal/mol K increments, cools down stepwise (5 steps, consisting of 500 t.u. each) to the production run simulation temperature with the equilibrated structure. The temperature is kept low for 10000 t.u. during which the DMD trajectory is captured. The DMD ensemble is clustered according to geometric similarity based on the Kabcsh RMSD for all pair-wise snapshot structures and by applying a hierarchical clustering algorithm [27,28]. For each cluster, both the structure closest to the centroid and the one with the lowest DMD energy are used as representatives for the QM phase.

Following DMD, the QM–DMD region is extracted from the centroid and lowest DMD energy structures. These structures undergo single point QM calculations, using BP86 [29–33] and a mixed double ζ quality basis set (def2-SVP) [34] for H, C, N, O, S, and a triple ζ quality basis set (def2-TZVPP) [35] for the metal [36]. To speed up the calculations, the Resolution of Identity (RI) [37], and Multipole Accelerated Resolution of Identity (MARI-J) [38] as implemented in *Turbomole* [39] were exploited. Empirical dispersion correction was included both in the energy and gradient evaluations [40]. Solvent was included via the Conductor-like Screening Model (COSMO) continuum solvent with the dielectric constant set to 20.0 [41], chosen as the best representation of the partially solvent-exposed active site of ARD [42]. Next, each structure is scored based on both the QM and DMD energies, and a single structure is selected from each iteration. The selected active site structure is partially optimized at the QM level, fixing the points of attachment to the rest of the protein. Lastly, the active site is reinstalled into the protein, and the QM–DMD boundary shrinks back to the QM-only and the simulation continues to the next DMD phase. The QM/DMD scheme propagates until convergence, based on the root-mean-squared-deviation (RMSD) of backbone Cα and QM and DMD energies. Simulations converged quickly (Figure 2B–D), within ca. 20 iterations, roughly corresponding to 10.5 ns of dynamics.

2.3. DFT mechanistic study

The QM/DMD simulations produce a set of well-equilibrated structures, of we which we chose the lowest QM energy structure to perform the mechanistic study. First, all stationary points along the reaction profile were calculated in an identical fashion: using the BP86 functional plus empirical dispersion correction, a double ζ quality basis set (def2-SVP) for H, C, N, O, S, a triple ζ quality basis set (def2-TZVPP) for cobalt and implicit solvation via COSMO with a dielectric of 20.0. BP86 is mentioned in a recent review [43] to give better energies for B_{12}-dependent enzymes that contain Co^{2+} when compared to B3LYP. In addition, TPSSh [44]/def2-TZVPP and B3LYP [45,46]/def2-TZVPP with empirical dispersion and implicit solvation were used to calculate the energies of the stationary points. Jensen et al. reported TPSSh is the most reliable choice of functionals for studying bioinorganic complexes [47]. The results reported in the main text are obtained with TPSSh, and those obtained with the BP86 and B3LYP functionals are given in the Supporting Information (Table S1). All intermediates were confirmed by having no imaginary frequencies, and transitions states having exactly one imaginary frequency in line with the reaction coordinate. However, in view of the constraints imposed by the position of the backbone of the protein, zero point energies were unrealistic and not added to the total energies computed. All charges were computed using Natural Population Analyses (NPA) [48] at the TPSSh/def2-TZVPP level of theory. We recognize the weakness of DFT when it comes to systems that exhibit spin cross over, however, with the size of our systems, we are limited to DFT and do believe we have captured the qualitative details of the system.

Mechanistic investigations were done on both low and high spin states of Co^{2+} structures generated from QM/DMD. Previous studies have shown that the low spin structures of Co^{2+} complexes are generally what exist in organometallic complexes and uniquely cobalamin, but high spin Co^{2+} exists for most natural metalloenzymes as shown by experiment and computation [49]. To include all possible spin combinations, the sextet adduct is calculated only in the mechanism and, as expected, too high in energy to be a viable catalytic option.

3. Results and discussion

3.1. Catalytic mechanism of doublet Co^{2+}

The lowest QM structure from the QM/DMD ensemble was selected and used in the mechanistic study. As with ARD/ARD′, the barrier toward dioxygen attack is not considered because the differences between ARD/ARD′ are rooted in later steps of the reaction profile.

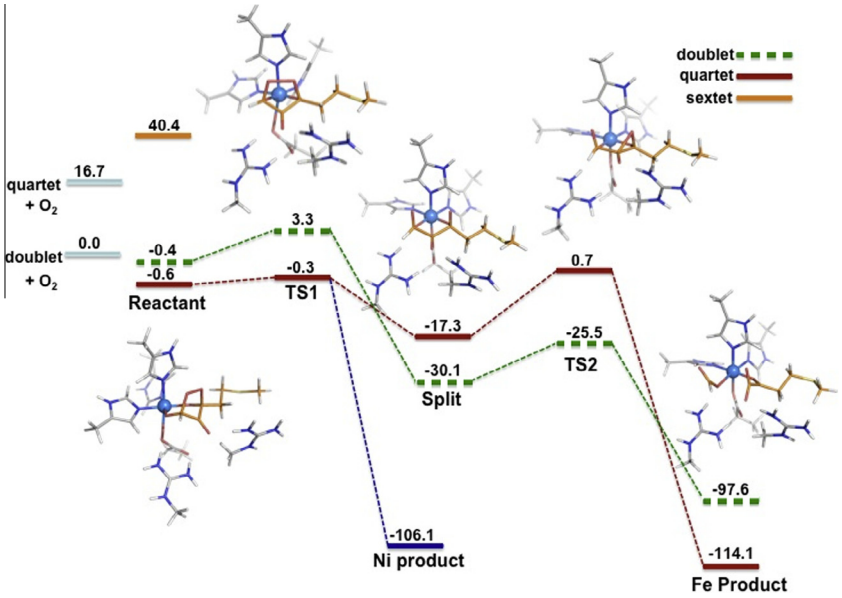

Figure 3. Catalytic mechanism of Co-ARD shows spin crossing at the dioxygen splitting and upon formation of the products (all relative energies reported in kcal/mol). A bifurcation in the PES is also found for the quartet system at TS1. All structures are optimized with BP86/def2-SVP (C, O, N, H) and def2-TZVPP (Co) with single point energies at TPSSh/def2-TZVPP.

For doublet Co^{2+}, the mechanism proceeds as follows: dioxygen binds to C1 and C3 of the substrate (see Figure 1 for atom labeling) and forms the dioxygen adduct with a negligible stabilization of the complex (0.4 kcal/mol). Next, the dioxygen separates with a barrier of 3.7 kcal/mol immediately into the split intermediate found in Fe-ARD′, where only the O–O bond is broken but the products are still coordinated to the metal. Following the split intermediate, O2 and C3 pass through an epoxy-like transition state of 4.6 kcal/mol and form the two products, formate and the α-keto acid. Doublet Co^{2+} was not observed to form Ni-ARD products upon the splitting of dioxygen (Figure 3).

3.2. Catalytic mechanism of quartet Co^{2+}

The quartet complex without dioxygen is substantially higher in energy (16.7 kcal/mol) then the doublet complex. However, upon dioxygen binding and formation of the adduct, the doublet (−0.4 kcal/mol) and quartet adduct (−0.6 kcal/mol) are essentially degenerate (Figure 3). Continuing along the path, the dioxygen splitting transition state (TS1) proceeds with a negligible barrier (0.3 kcal/mol) into the Ni-ARD products. However, TS1 sits at an unexpected bifurcation in the PES, where the reaction has the choice to either proceed directly to the oxidation of the substrate to Ni-ARD products, or continue along the Fe-ARD′ pathway. Following the O–O bond split, we are able to capture the thermodynamically preferred Ni-ARD products. However, proceeding through to the split intermediate into the Fe-ARD′ products is still energetically very favorable, through the epoxy-like TS2 with a barrier of 18.0 kcal/mol. The kinetics of this bifurcation and the resultant ratio of the forming products cannot be assessed without the use of on-the-fly dynamics, and this system is indeed interesting for the future dynamics study.

Table 1
Natural Population Analysis (NPA) charges are listed for residues H96, H98, D102, H140, the substrate, dioxygen and the metal for all stationary points along the reaction path for low spin Co-ARD (top row, bold), high spin Co-ARD (second row, bold and italicized) and Fe-ARD′ (third row). When comparing all the charges from the reactants' stationary point to the split intermediate, an overall trend of increasing positive charge on all the residues and the negative change on O_2 can be seen. Charges were taken from structures optimized at BP86/def2-SVP (H, C, O, N, H) and def2-TZVPP (Co) and singles points taken at TPSSh/def2-TZVPP.

	H96	H98	D102	H140	R104	R154	Substrate	O_2	Co^{2+}
Reactant	**0.08**	**0.14**	**−0.82**	**0.17**	**0.85**	**0.96**	**−0.83**	**−0.65**	**1.09**
	0.05	***0.04***	***−0.85***	***0.08***	***0.90***	***0.99***	***−1.04***	***−0.65***	***1.48***
	0.08[a]	0.07	−0.82	0.06	0.88	0.94	−1.00	−0.66	1.46
TS1	**0.08**	**0.14**	**−0.82**	**0.17**	**0.85**	**0.97**	**−0.80**	**−0.68**	**1.09**
	0.06	***0.05***	***−0.86***	***0.08***	***0.90***	***0.99***	***−1.02***	***−0.65***	***1.46***
	0.08	0.07	−0.82	0.06	0.88	0.94	−0.98	−0.68	1.45
Split	**0.28**	**0.26**	**−0.67**	**0.26**	**0.92**	**0.94**	**−0.73**	**−1.36**	**1.10**
	0.11	***0.22***	***−0.78***	***0.22***	***0.82***	***0.95***	***−0.47***	***−1.47***	***1.40***
	0.13	0.15	−0.79	0.15	0.90	0.94	−0.66	−1.30	1.48
TS2	**0.27**	**0.26**	**−0.65**	**0.28**	**0.92**	**0.91**	**−0.75**	**−1.33**	**1.10**
	0.13	***0.15***	***−0.77***	***0.14***	***0.80***	***0.94***	***−0.51***	***−1.46***	***1.59***
	0.13	0.16	−0.79	0.16	0.90	0.93	−0.65	−1.34	1.50
Product (Fe)	**0.17**	**0.10**	**−0.78**	**0.23**	**0.91**	**0.92**	**−0.21**	**−1.41**	**1.08**
	0.09	***0.08***	***−0.83***	***0.11***	***0.86***	***0.92***	***−0.29***	***−1.41***	***1.47***
	0.07	*	−0.81	0.09	0.90	0.92	−0.33	−1.41	1.47
Product (Ni)	*	*	*	*	*	*	*	*	*
	0.09	***0.01***	***−0.82***	***0.08***	***0.88***	***0.91***	***−0.19***	***−1.45***	***1.50***

[a] Values are taken from Ref. [2].

3.3. Unique split dioxygen intermediate in low and high spin Co^{2+}-ARD

The split dioxygen intermediate found in both low and high spin Co-ARD was first observed in Fe-ARD. To compare these intermediates to the Fe-ARD one, NPA calculations of partial charges are computed for all lowest energy stationary points for both spin states of Co (Table 1, listed in order of low spin Co-ARD, high spin Co-ARD and Fe-ARD′). If you follow the NPA charges of all the residues coordinating the metal, substrate and dioxygen throughout the duration of the mechanism, there are several charges to take note of: (1) Upon formation of the split dioxygen intermediate and into the epoxy-like transition state, the coordinating residues (H96, H98, D102 and H140) become more positively charged. The electrons withdrawn from these residues flow through the Co metal center and donate electron density to the $\pi*$ orbital of dioxygen, stabilizing the split intermediate. (2) Although the metal facilitates the flow of electron density as a RedOx flexible center, it does not change oxidation state throughout the reaction profile.

Comparing bond distances of the two spin states of Co-ARD, overall low spin Co has shorter metal–ligand bond distances than high spin Co complexes. The low spin adduct has Co–O1 and Co–O3 bond distances of 1.93 and 1.91 Å, respectively. For high spin Co, the bond distances are 2.10 and 1.97 Å, respectively. The shorter bond distances of low spin Co adduct are comparable to the longer metal–ligand distances observed in Fe-ARD′ (1.91 and 1.93 Å, respectively) giving the low spin Co-ARD a stronger and more RedOx active interaction. The longer bond distances of high spin Co are similar to the ones found in Ni-ARD (2.19 and 2.00 Å, respectively). These longer bond distances could be a contributing factor in high spin Co-ARD bifurcation PES. Co can play the role of a Lewis acid, coordinating and polarizing the substrate without any RedOx activity, or Co can play an active role as a RedOx flexible metal and pass through the split intermediate into the Fe-ARD′ products.

The two spin states considered here (starting from the complexes of the protein with the substrate and dioxygen bound) yield very accessible reaction profiles that are nearly-degenerate in the area of TS1, and go down-hill from there. Both Ni-ARD and Fe-ARD′ products are predicted from our simulations for Co^{2+}-dependent ARD. Our calculations may not have recognized the high spin route as the exclusive option since we do not have the spin crossing profile and do not consider the dioxygen attachment to the substrate forming the adduct. However, we do see that the high spin Co profile does form Ni products very efficiently, which has been shown in experiments. The presence of spin cross-over between the doublet and quartet is evident but something we are not able to address because of prohibitively high computational cost. It is also possible that the Co-ARD mechanism is kinetically driven.

4. Conclusions

The pair of acireductone dioxygenases, ARD′ and ARD, facilitate the recycling of methionine in cells when Fe^{2+} is present within the active site or exit the pathway entirely when Ni^{2+} is present. Our previous study explicated the mechanism behind this long-standing mystery, showing that the metal solely dictates the mechanism through the degree of charge transfer to dioxygen in the reaction, linked to the RedOx flexibility of the metal. This purely metal-dependent functionality led to exploring how Co, the element in between Fe and Ni, oxidizes the substrate, 1,2-dihydroxy-3-keto-5-(methylthio)pentene. Through mixed quantum–classical dynamics simulations using our QM/DMD method, and subsequent DFT mechanistic studies, we showed here that low spin Co^{2+} PES exclusively follows the Fe^{2+}-dependent pathways, producing α-keto acid precursor of methionine and formate, while the high spin Co^{2+} PES contains a bifurcation in the pathway that follows along both the Fe^{2+}-dependent pathway and Ni^{2+}-dependent pathway that produces methylthiopropionate, carbon monoxide and formate. Thus Co-ARD should be able to produce both sets of products, partially working as an intermediate form between ARD and ARD′. The resultant product distribution could be accessed through dynamics studies of the complete reaction path, but this remains to be done in the future.

Acknowledgements

This work was supported by the DARPA Young Faculty Award N66001-11-1-4138 (A.N.A.), The Alfred Sloan Fellowship (A.N.A.) and the NSF Graduate Fellowship #2011115747 (C.E.V.).

Appendix A. Supplementary data

Supplementary data associated with this article can be found, in the online version, at http://dx.doi.org/10.1016/j.cplett.2014.04.055.

References

[1] S.J. Lippard, J.M. Berg, Principles of Bioinorganic Chemistry, University Science Books, Mill Valley, California, 1994.
[2] M. Sparta, C.E. Valdez, A.N. Alexandrova, J. Mol. Biol. 245 (2013) 3007.
[3] W.R. Myers, J.W. Wray, S. Fish, R.H. Abeles, J. Biol. Chem. 268 (1993) 24785.
[4] S.W. Oram et al., Neoplasia 9 (2007) 643.
[5] M.J. Maroney, S. Ciurli, Chem. Rev. (2013), http://dx.doi.org/10.1021/cr4004488.
[6] I. Bertini, H.B. Gray, E.I. Stiefel, J.S. Valetine, Biological Inorganic Chemistry: Structure and Reactivity, University Science Books, 2007.
[7] P. Carloni, F. Alber, D. Sebastiani, U. Rothlisberger, Advances in density-functional-based modeling techniques – recent extensions of the Car-Parrinello approach, in: Quantum Medicinal Chemistry, Wiley-VCH, Weinheim, Germany, 2003, pp. 5–36.
[8] L.A. Eriksson, Theoretical Biochemistry: Processes and Properties of Biological Systems, Elsevier Science B.V., 2001.
[9] S. Lindskog, Cobalt (II) in metalloenzymes. A reporter of structure-function relations, Springer, Berlin, Germany, 1970, pp. 153–196.
[10] D.R. McMillian, R.C. Rosenberg, H.B. Gray, Proc. Nat. Acad. Sci. USA 71 (1974) 4760.
[11] Y. Dai, P.C. Wensink, R.H. Abeles, J. Bio. Chem. 274 (1999) 1193.
[12] Y. Dai, T.C. Pochapsky, R.H. Abeles, Biochemistry 40 (2001) 6379.
[13] T. Ju, R. Goldsmith, S. Chai, M.J. Maroney, S.S. Pochapsky, T.C. Pochapsky, J. Mol. Biol. 393 (2006) 823.
[14] F. Al-Mjeni, T. Ju, T.C. Pochapsky, M.J. Maroney, Biochemistry 41 (2002) 6761.
[15] T.C. Pochapsky, T. Ju, M. Dang, R. Beaulieu, G.M. Pagani, B. OuYang, Metal Ions in Life Sciences, vol. 2, Wiley-VCH, Weinheim, Germany, 2007, pp. 473–500.
[16] W.J. Wray, H.R. Abeles, J. Biol. Chem. 270 (1995) 3147.
[17] N.V. Dokholyan, S.V. Buldyrev, H.E. Stanley, E.I. Shakhnovich, Fold Des. 3 (1998) 577.
[18] N.V. Dokholyan, Curr. Opin. Struct. Biol. 16 (2006) 79.
[19] F. Ding, W.H. Guo, N.V. Dokholyan, E.I. Shakhnovich, J.E. Shea, J. Mol. Biol. 350 (2005) 1035.
[20] F. Ding, D. Tsao, H. Nie, N.V. Dokholyan, Structure 16 (2008) 1010.
[21] M. Sparta, F. Ding, D. Shirvanyants, N.V. Dokholyan, A.N. Alexandrova, Biophys. J. 103 (2012) 767.
[22] C.E. Valdez, A.N. Alexandrova, J. Phys. Chem. B. 116 (2012) 10649.
[23] H.M. Senn, W. Thiel, Angew. Chem. Int. Ed. Engl. 48 (2009) 1198.
[24] C.E. Valdez, M. Sparta, A.N. Alexandrova, J. Chem. Theory Comput. 9 (2012) 730.
[25] M. Sparta, A.N. Alexandrova, PLoS One 7 (2012) e47172.
[26] H.C. Andersen, J. Chem. Phys. 72 (1980) 2384.
[27] W. Kabsch, Acta Crystallogr. A 32 (1976) 922.
[28] Barton, G. J. OC – A cluster analysis program, University of Dundee, Scotland, UK (1993, 2002). <www.compbio.dundee.ac.uk/downloads/oc>.
[29] P.A.M. Dirac, Proc. R. Soc. London, Ser. A 123 (1929) 714.
[30] J.C. Slater, Phys. Rev. 81 (1951) 385.
[31] S.H. Vosko, L. Wilk, M. Nusair, Can. J. Phys. 80 (1980) 1200.
[32] A.D. Becke, Phys. Rev. A 38 (1998) 3098.
[33] J.P. Perdew, Phys. Rev. B 33 (1986) 8822.
[34] A. Schafer, H. Horn, R. Ahlrichs, J. Chem. Phys. 97 (1992) 2571.
[35] F. Weigend, R. Ahlrichs, Phys. Chem. Chem. Phys. 7 (2005) 3297.
[36] Y. Yang, M.N. Weaver, K.M. Merz, J. Phys. Chem. A 113 (2009) 9843.

[37] M.V. Arnim, R. Ahlrichs, J. Comput. Chem. 19 (1998) 1746.
[38] M. Sierka, A. Hogekamp, R. Ahlrichs, J. Chem. Phys. 118 (2003) 9136.
[39] Turbomole V6.3 2011, a development of University of Karlsruhe and Forschungszentrum Karlsruhe GmbH, 1989-2007, Turbomole GmbH, since 2007. Available from: <http://www.turbomole.com>.
[40] S. Grimme, J. Comput. Chem. 25 (2004) 1463.
[41] A. Klamt, G.J. Schüürmann, J. Chem. Soc. Perkin Trans. 2 (5) (1993) 799.
[42] P.E.M. Siegbahn, M.R.A. Blomberg, Chem. Rev. 100 (2000) 421.
[43] M.R.A. Blomberg, T. Borowski, F. Himo, R. Liao, P.E.M. Siegbahn, Chem. Rev. 114 (2014) 3601–3658.
[44] V. Staroverov, G. Scuseria, J. Tao, J. Perdew, J. Chem. Phys. 119 (2003) 12129.
[45] A.D.J. Becke, Chem. Phys. 98 (1993) 5648.
[46] S. Grimme, J. Antony, S. Ehrlich, H. Krieg, J. Chem. Phys. 132 (2010) 154104.
[47] K.P. Jensen, Inorg. Chem. 47 (2008) 10357.
[48] A.E. Reed, R.B. Weinstock, F. Weinhold, J. Chem. Phys. 83 (1985) 735.
[49] K.O. Jensen, U. Ryde, J. Mol. Struct.: THEOCHEM 585 (2000) 239.